

# Distribution of PM<sub>10</sub>, PM<sub>2.5</sub>, and NO<sub>2</sub> in the Cergy-Pontoise urban area (France)

Souad Lagmiri | Salem Dahech

Department of Geography, Paris Cité University, UMR PRODIG, Paris, France

## Correspondence

Souad Lagmiri, Research Center for the Organization and Dissemination of Geographic Information (PRODIG), UMR 8586 (CNRS), Paris City University, 75013 Paris, France.

Email: [souad.lagmiri@gmail.com](mailto:souad.lagmiri@gmail.com)

## Funding information

Cergy-Pontoise Conurbation; French Ministry of Higher Education and Research

## Abstract

This study employed a network comprising 16 fixed “Ecosmart” sensors deployed in the Cergy-Pontoise conurbation. Continuous measurements of PM<sub>10</sub>, PM<sub>2.5</sub>, and NO<sub>2</sub>, significant pollutants in the Paris region, were conducted from April 8 to June 6, 2022. The collected data were represented as statistically composite spatial matrices due to the heterogeneous urban landscape and the overlapping of multiple pollution sources. Temporal variations on a daily basis were influenced by both traffic and meteorological conditions. Daytime, characterized by denser traffic compared to nighttime, exhibited higher concentrations of PM<sub>10</sub> and PM<sub>2.5</sub>. Conversely, NO<sub>2</sub> concentration levels displayed two peaks associated with traffic volume, and relatively elevated nocturnal values compared with midday due to atmospheric vertical stability during the nighttime phase. The analysis of weather-type impacts revealed that during unstable weather conditions, elevated particle concentrations stemmed from dust resuspension from the ground and long-range transport. Maximum NO<sub>2</sub> concentrations were observed during stable weather conditions, whereas minimum concentrations occurred during unstable weather.

## KEY WORDS

air quality, fixed stations, GIS, spatiotemporal distribution, statistics, urban forms, weather types

## 1 | INTRODUCTION

The technological innovations developed in recent decades have contributed to urban expansion, resulting in social and economic transformations of cities. Urban dynamics have, in some aspects, significantly improved the living conditions of populations, but certain models of urbanization have proven to be incompatible in the long term for a good quality of life. This threat particularly affects air quality, the degradation of which poses a major risk to the health of city dwellers (Krewski

et al., 2009; Weinmayr et al., 2015; Xing et al., 2016). Due to this impact, continuously monitoring air quality has become one of the main sustainable development goals (SDG). For this purpose, several air quality monitoring instruments have been installed in urban areas. Directive 2008/50/EC on ambient air quality has defined the minimum number of air quality monitoring stations (AQMS) based on population density. Usually, an official AQMS covers an average of about 100,000 people in cities of developed countries. However, this distribution is insufficient to obtain accurate information on the spatial

This is an open access article under the terms of the [Creative Commons Attribution-NonCommercial](#) License, which permits use, distribution and reproduction in any medium, provided the original work is properly cited and is not used for commercial purposes.

© 2024 The Author(s). *Meteorological Applications* published by John Wiley & Sons Ltd on behalf of Royal Meteorological Society.

distribution of emissions and to identify their sources (Hoek et al., 2008). Some researchers have implemented personal measurements to compensate for the insufficiency of conventional measurements. Other studies have explored the potential of simulation software to predict pollution under different scenarios (Balczó et al., 2009; Bozó et al., 2006; Jonhson et al., 2010; Liu et al., 2012; Misra et al., 2019; Naughton et al., 2018; Pepe et al., 2016; Weidinger et al., 2010; Xing et al., 2015). Ung (2003) opted for using modeling to create “virtual stations,” as a means of artificially densifying the measurement network. He successfully simulated air pollution on a scale ranging from 10 m to 10 km. However, this system has limitations mainly due to the need for regular data updates provided by multidisciplinary teams to establish a coherent coupling platform.

Like all conurbations in the Ile de France region (in France), Cergy-Pontoise occasionally experiences atmospheric pollution episodes. Its urban environment has been changing for over 25 years. Currently, 61% of the Cergy-Pontoise Agglomeration Community (CPAC) space is urbanized (+13% between 1990 and 2021), mainly in the city centers of this conurbation where medium and low-income populations reside. With over 210,000 inhabitants (INSEE, 2019), it has experienced a demographic growth of approximately 16% since the early 2000s. The conurbation consists of 13 contiguous municipalities marked by economic, social, and environmental interdependence, with Cergy and Pontoise being the two main cities. The city centers are relatively compact. The predominant land use is residential, mainly concentrated in the central and eastern parts of the conurbation (for more details regarding the study area, refer to our article: Lagmiri & Dahech, 2023). The CPAC has a household car ownership rate of 80.8%. Thanks to its location as an interface between Paris and Western France, the CPAC benefits from its geographical position, attracting businesses that establish and grow there. Currently, there are 20 business parks covering over 1080 ha, which represents 14% of its territory. They accommodate 14,000 companies generating 90,500 jobs (IAU, 2019), with 54% of employees working in establishments with over 100 employees. When the number of vehicles of employees commuting to work on-site exceeds 500 units per day, a significant number of these establishments are considered major “traffic generators” (PPA, 2013). From a qualitative standpoint, it can be assumed that air quality is more degraded in the activity zones and the central and eastern parts of the conurbation. To verify this hypothesis, it would be interesting to measure the concentrations of air pollutants at various sites based on traffic density and land use. To date, only one air quality monitoring station, operated by AirParif—the association

responsible for air quality measurements in the Île-de-France region—is installed on the CPAC territory. The station conducts continuous PM<sub>10</sub> measurements and provides very accurate information, but at a very low spatial resolution, making it difficult to make decisions regarding certain areas distant from the station. Monitoring of nitrogen dioxide (NO<sub>2</sub>) concentrations was conducted only once and for a short duration (November 13 to December 11, 2018). It was carried out using mini-sensors mounted on a set of lampposts. These sensors provided NO<sub>2</sub> measurements that exceeded the limit values set by the European Commission on Air Quality. This measurement campaign was conducted at a single sampling site on the edge of a busy road (Boulevard de la Viosne in Cergy), implying that the observed NO<sub>2</sub> levels were specific to the site and did not characterize the spatial distribution in the conurbation.

Since the primary pollutant emissions (NO<sub>2</sub>, PM<sub>10</sub>, and PM<sub>2.5</sub>) are not homogeneous in the CPAC, and the degree of dispersion depends on the influence of land use and weather types, no effective pollution reduction measures can be conducted without prior research on the spatiotemporal variability of air quality. To ensure better spatial coverage, the present study uses a network of 16 fixed outdoor air pollution monitoring stations of the “Ecosmart” type to provide precise information. This is the first attempt at multisite and long-term measurements of pollutants NO<sub>2</sub>, PM<sub>10</sub>, and PM<sub>2.5</sub> in an urban area designed (1968) specifically to counterbalance the “uncontrolled urban sprawl” of Paris. The measurements carried out by this fixed network allow, in the first instance, to identify the factors influencing the spatiotemporal variability of pollution. In the second instance, our study focuses on the analysis of different weather types as major contributing factors to the temporal variation of NO<sub>2</sub>, PM<sub>10</sub>, and PM<sub>2.5</sub> pollutants. Previous works on weather types have concluded that the state of the atmosphere plays a role in the dispersion or accumulation of pollutants near the surface. They explain that pollutants rise in the air due to buoyancy conditions (convection) and disperse horizontally and vertically due to mechanical turbulence. The works of Dahech et al. (2022), Lagmiri and Dahech (2023), and Sindosi et al. (2003) can be cited as examples of an applied analysis of the impact of weather types on air pollution.

## 2 | DATA AND METHODS

### 2.1 | Monitoring network

A network consisting of 16 pollution measurement stations is installed on the CPAC territory from April



**FIGURE 1** Pictures of installations in an urban center, a residential site, a rural environment, and an urban park, taken during the sensor installation campaign on March 26, 2022.

8, 2022. It continuously monitors the concentrations of gases and particles ( $\text{NO}_2$ ,  $\text{PM}_{10}$ ,  $\text{PM}_{2.5}$ ) using a chemiluminescence component for the former and an optical component for the latter. These components offer numerous advantages. They react quickly to changes in pollutant concentrations and are not affected by humidity, which maximizes the sensor's reliability. Each station also includes a component to detect meteorological parameters (temperature, humidity, and pressure) and includes a SIM card for cellular communication via the 4G network. The sensors are designed to operate on a 5VDC power supply. In this study, they are powered by electricity from public grid, using AC/DC converters (Figure 1). These sensors are installed on public lighting poles and thus powered when public lighting is active. In the absence of electrical power, which is systematically cut during the day, they are automatically powered by an integrated backup battery that provides electrical autonomy throughout the day. All these components are housed in a ventilated enclosure to increase air renewal rates. The enclosure is mounted 3 m above the ground to avoid acts of vandalism and to measure ambient air pollution while avoiding certain point source emissions (vehicle exhausts, tobacco, etc.).

The measurements are taken every minute and transmitted in real time to a web server. The web server used is multitasking. It allows remote management of meteorological and air pollution parameters (sampling frequency change, addition/removal of parameters, unit change), provides reports, performs data storage and on-screen display in the form of graphs, and enables programming of alerts in case of exceeding certain thresholds. The sensors are calibrated using analyzers approved by the LCSQA (Central Laboratory for Air Quality Monitoring) and verified annually according to ISO 17025 standards (Thermo Scientific T42i for NO and  $\text{NO}_2$ ; Palas Fidas 200 and Thermo Scientific TEOM 1405 for particulate matter measurement; Thermo Scientific 146iQ for multi-gas calibration). Calibration involves adjusting the parameters of each sensor to best match the sensor's response with the actual concentration measured by the reference analyzers (Figure 2). The calibration process is automated using a multipoint approach to ensure better accuracy and consistency of sensor measurements. It is achieved through various algorithms that account for temperature and pressure drifts. Regarding verification, the sensors are positioned side by side to assess the consistency of measurements between the devices.

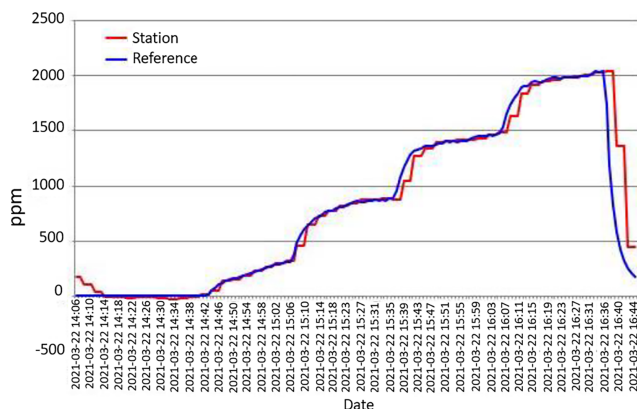


**FIGURE 2** Comparison of various  $\text{PM}_{2.5}$  sensors with a TEOM1405 in an outdoor environment; on the right, a graph illustrating the results of this comparison.

	Scale	Detection limit	Precision
$\text{NO}_2$ sensor (electrochemical)	0–5000 ppb	3 ppb	3 ppb
$\text{PM}_1$ , $\text{PM}_{2.5}$ and $\text{PM}_{10}$ sensor (optical)	0–1000 $\mu\text{g}/\text{m}^3$	2 $\mu\text{g}/\text{m}^3$	4 $\mu\text{g}/\text{m}^3$
Temperature	–20–+50°C		0.3°C
Humidity	0%–100%		2%
Pressure	300–1100 hPa		1 hPa

**TABLE 1** Performance of measurements of components included in the sensor.

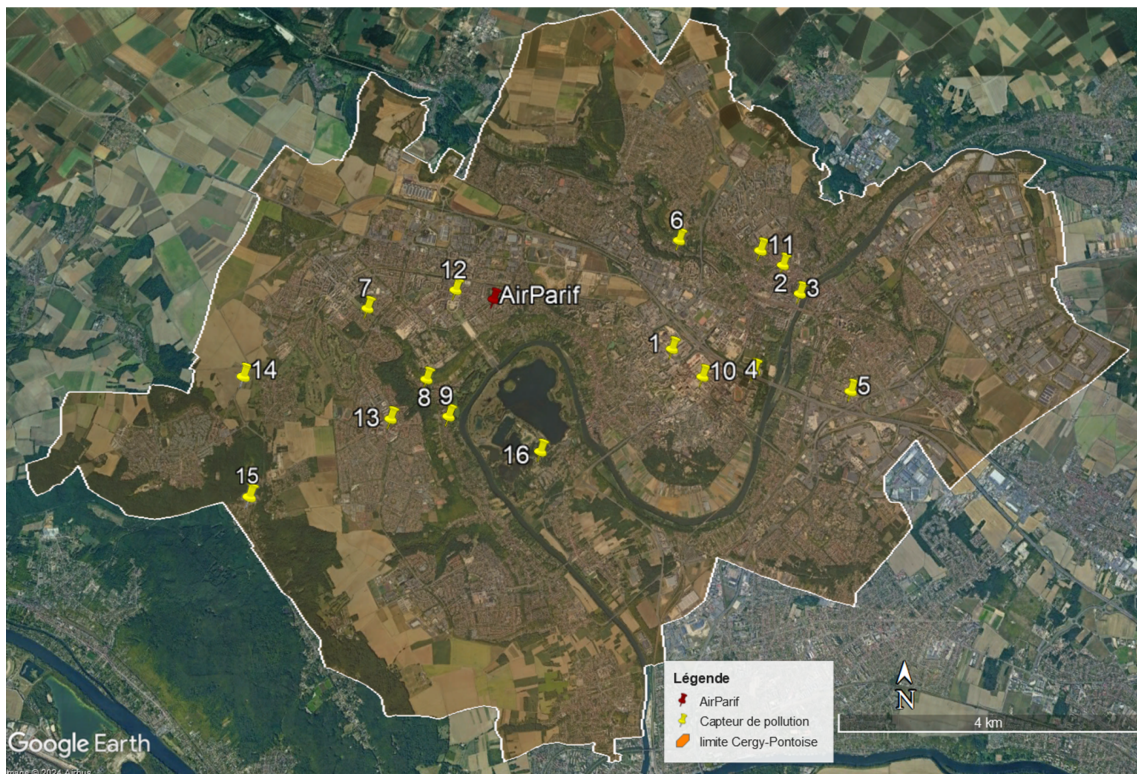


**FIGURE 3** Location of the 16 pollution sensors in the Cergy-Pontoise conurbation ( $89 \text{ km}^2$ ) in yellow and the reference station AirParif in red.

TABLE 2 Types of stations as suggested by AirParif and the characteristics of each sampling site.

Station number	Station type	Altitude (m)	Street type	Features
A1	Downtown	52	On the university campus	Located 77 m from the intersection of two 4-lane roads and 380 m from the “a15” highway ring road. The speed is limited to 50 km/h. Buildings are mostly six stories. Presence of construction sites.
A2	Downtown	52	5.61-m-wide one-way road	Speed not exceeding 10 km/h. A large attendance of the population. Absence of vegetation.
A3	Downtown	28	12.68-m-wide two-way road	Close to the Oise River. Dense traffic with a speed of 50 km/h. A few trees lined up.
A4	Sports complex (near a high-traffic road)	45	4-lane highway “a15”	Separated from the “a15” highway by a strip of lined trees
A5	Suburban collective housing	42	9.4-m-wide two-way road	Located in a peripheral area with collective buildings and 61 meters from the interchange between the “A15” highway (8 lanes) and the N184 national road (4 lanes). The district is separated from the interchange by a nearly 6-meter-high wall.
A6	Suburban residence	44	9.62-m-wide two-way road	On a large depression with vegetation. Speed is limited to 30 km/h.
A7	Suburban residence	111	7.89-m-wide two-way road	Close to green space
A8	Suburban residence	45	3.57-m-wide one-way road	Wooded site enclosed by two slopes. Close to the Oise River and the urban park. Traffic is exclusively for residents with a speed limit of 10 km/h.
A9	Suburban residence	37	3.91-m-wide one-way road	Located on a slope with significant vegetation. Close to the Oise River and the urban park. Moderate to low traffic with a speed limit of 50 km/h.
A10	Downtown	49	Bus square. Two-way traffic on a 32.82-m-wide road.	Cergy city center. Heavy traffic and pedestrian flow. The speed is limited to 30 km/h. Presence of buildings mainly with 6 floors. Presence of construction sites.
A11	Downtown	39	The intersection of three one-way roads	Speed is limited to 10 km/h. Building in height. Presence of a few trees. Significant attendance by the population.
A12	Downtown	107	Place at 23.17-m-wide. Presence of a 6.08-m-wide two-way road.	Speed is limited to 10 km/h. Collective buildings. A place without vegetation. Marketplace twice a week. Located 634 m from the urban park.
A13	Downtown	99	Roundabout	Located 450 m from the wood
A14	Rural	125	7-m-wide two-way road	A rural area located in the direction of the prevailing northwest wind. Vast agricultural field.
A15	Rural residence	191	The road is 5.67 m wide	Rural neighborhood in the middle of the forest. Traffic exclusively for residents.
A16	Urban park	26		Located in depression. Presence of a large lake and a river. Presence of significant vegetation. High attendance of visitors during sunny days.

During an intercomparison campaign conducted by the Central Air Quality Monitoring Laboratory (LCSQA), this equipment stood out from other tested systems for its performance, reliability, and ease of implementation (Spinelle et al., 2020). The performance of these sensors is illustrated in Table 1.

## 2.2 | Sampling sites

The measurement stations are all installed on lampposts along the immediate edge of the roads, except for two stations; A16, which is installed in the middle of a park, and A10, which is installed 77 meters away from the road.

The network is distributed in such a way that it covers a diversity of urban landscapes in the conurbation (Figure 3). Representative urban areas have been selected: seven sites in the city center and six in peripheral residential areas. The remaining three sites are distributed between an urban park, a rural area, and a rural residence. These sites are characterized by differences in construction type, visitor density, percentage of greenery, street layout, density, and speed of traffic. The characteristics of the different zones are summarized in Table 2.

## 2.3 | Statistical data processing

Urban heating systems, often fueled by fossil fuels such as natural gas, can emit pollutants such as nitrogen oxides ( $\text{NO}_x$ ) and fine particles. The study period for this work, from April 8 to June 6, 2022, coincides with a reduction in urban heating activity. Consequently, the detected pollution primarily originates from natural sources such as dust transport (Euphrasie-Clotilde, 2018; Lasserre, 2006; Prospero et al., 1981), as well as from road traffic, emanating from exhaust systems and the resuspension of particles into the air through the mechanical action of wheels (Alary et al., 1995; Carteret et al., 2014; Nicolas, 1996). The pollutants  $\text{NO}_2$ ,  $\text{PM}_{10}$ , and  $\text{PM}_{2.5}$  are continuously measured at a temporal resolution of 1 min. After a statistical check, we identified a 5% of missing data, amounting to 67,115 values, in a series of 1,345,568 records. These missing values occur primarily as an instantaneous loss of measurements (from 1 to 3 min) or sometimes as a sequence of several consecutive minutes without exceeding an average of 13 min per sequence. They are related to a power supply or cellular communication failure between the automated stations and the web server. The missing data have been estimated using the corresponding hourly averages. The rural station was treated separately because it is characterized by an almost absence of measurements from 6 to 8 p.m. This discontinuity is linked to the lighting rhythm in the uninhabited rural area. Once the chronological series is complete, a preprocessing based on calculating the median value for each hour is carried out to eliminate very low values and instantaneous peaks. This step is essential for accurately calculating the hourly trends and creating a reliable database for this study.

For an objective interpretation of the spatiotemporal distribution of air pollution, a hierarchical Ascending Classification (HAC) was conducted. Sites with similar pollution patterns are grouped using Ward's method, known for its sensitivity to hierarchical structures and linear relationships among variables. It is particularly effective at capturing variance or covariance structures in

the data, distinguishing it from other methods. The Euclidean distance is the chosen algorithm for this classification to maximize attribute homogeneity within groups and heterogeneity between groups. The aim is to determine the best spatial grouping of sampling sites to objectively reveal possible differences and similarities between them. The method used in the document is not proposed as a substitute for the subjective comparison systems between sites practiced in many studies (Dahech, 2007b; Wolf-Benning et al., 2009) but as a complement to existing methods.

The spatial clustering results of the sampling sites are then used as inputs, on one hand, in the Kolmogorov-Smirnov (K-S) test to verify the statistical normality of the distribution, and on the other hand, in the Kruskal-Wallis test, to check the spatial variability. All these statistical treatments are performed using the SPSS software. Geographic information systems (GIS) are used to visualize the spatial distribution of average concentrations. The results of the temporal distribution are presented on a time scale ranging from hourly to weekly. They are interpreted based on the impact of anthropogenic and natural factors on pollutant concentrations.

To assess the impact of weather types, we carried out a simple statistical description of the concentrations recorded during stable weather (atmospheric pressure  $>1015$  hPa, wind speed  $<5$  m/s, and cloud cover  $<2$  octas) and during unstable weather (atmospheric pressure  $<1010$  hPa, wind speed  $>5$  m/s, and cloud cover  $>6$  octas). These two weather types are identified using meteorological data recorded by the "Cormeilles en Vexin" weather station, located 15 km from the study area, as well as surface and upper-level atmospheric pressure maps (geopotential 500 hPa) from the global forecasting system (GFS), archived on the webpage (Wetterzentrale.de).

## 3 | RESULTS

### 3.1 | Air quality overview from April to early June

The HAC using the Ward method was applied to a database consisting of 16 columns (16 stations) and 1417 rows (1417 hourly series of pollutant concentrations) for the selected period in this study and for each pollutant. It should be noted that no distinction between weather types was made in this classification. This process resulted in the identification of five clusters for  $\text{NO}_2$  and  $\text{PM}_{2.5}$ , and four clusters for  $\text{PM}_{10}$ , each showing a high level of spatial homogeneity (Figure 4). The composition of the clusters by site category reveals

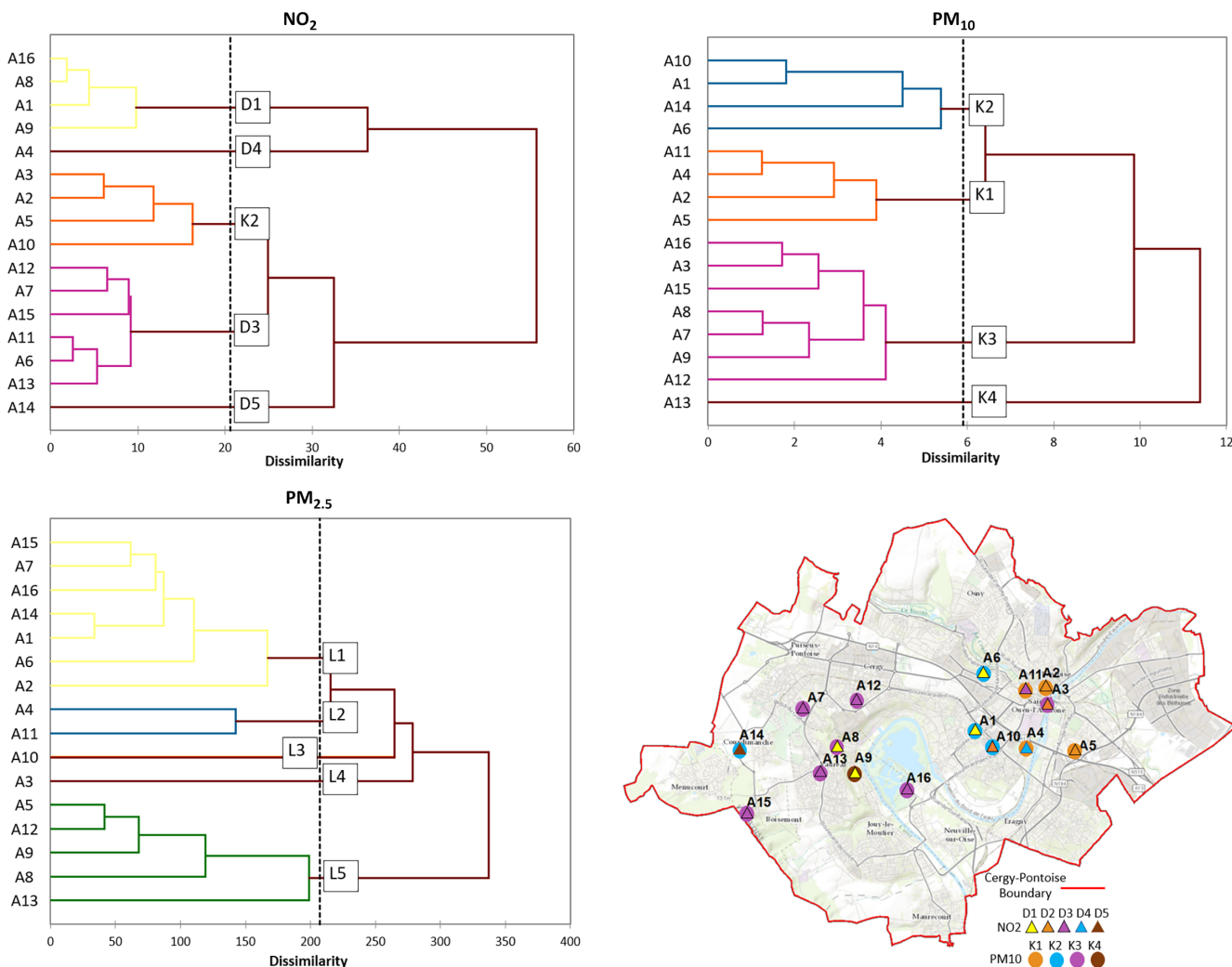


**FIGURE 4** Dendograms (NO<sub>2</sub>, PM<sub>10</sub> and PM<sub>2.5</sub>) showing the spatial classification of air quality monitoring sites and map of the spatial distribution of station clusters for NO<sub>2</sub> and PM<sub>10</sub> (data from April 8 to June 6, 2022).

that PM<sub>10</sub>, PM<sub>2.5</sub>, and NO<sub>2</sub> do not primarily originate from the same source or the dispersion conditions act differently.

### 3.1.1 | Normality test

The Kolmogorov-Smirnov normality test was conducted to statistically examine the spatial variability of air quality throughout the study period. Kolmogorov-Smirnov test was chosen because it is suitable for large samples, unlike the Shapiro-Wilk test, which is appropriate for small samples. The results of this test are reported in Table 3. They show that for all pollutants, the “*p*” value is below the acceptable level of significance set at 0.05, and there is a significant maximum cumulative distance between the histogram of the measured data and the corresponding Gaussian distribution curve. This indicates

that the concentrations in different groups do not follow a normal distribution. In this case, the nonparametric independent Kruskal-Wallis test is preferred to assess spatial heterogeneity (Table 3). With a *p*-value of zero (*p* < 0.05) for this test, all spatial series have been found to exhibit statistically significant variability. This result could most likely be explained by the distribution of emission sources and the specific topography of the sampling sites.

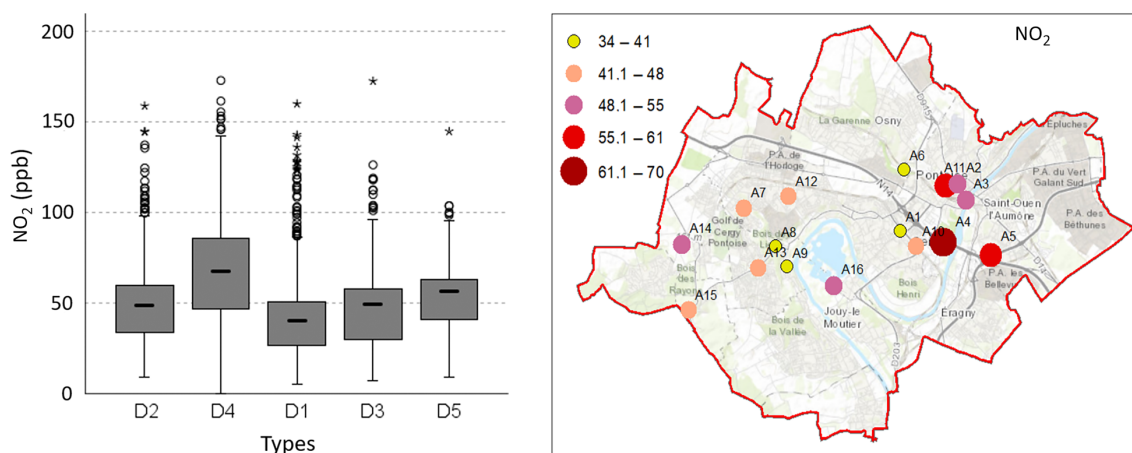
### 3.1.2 | Distribution of nitrogen dioxide pollution

The pollution measurement stations are located in the Cergy-Pontoise urban area, directly along the roads. Since road traffic is one of the main sources of NO<sub>2</sub>, all measurements reveal exceedances of WHO standards

**TABLE 3** Results of the Kolmogorov–Smirnov test and Kruskal–Wallis test (mean and standard deviation [SD]).

Pollutant	ID	Mean $\pm$ SD	Distance K-S	p-Value Kolmogorov–Smirnov	p-Value Kruskal–Wallis
$\text{NO}_2$ (ppb)	D1	$40.38 \pm 18.25$	3.4	0.000	0.000
	D2	$49.41 \pm 20.06$	2.3	0.002	
	D3	$46.99 \pm 19.46$	3.4	0.000	
	D4	$69.64 \pm 27.23$	0.7	0.005	
	D5	$52.53 \pm 16.7$	2.4	0.000	
$\text{PM}_{10}$ ( $\mu\text{g}/\text{m}^3$ )	K1	$19.28 \pm 16.18$	5.1	0.000	0.000
	K2	$31.96 \pm 30.68$	4.2	0.001	
	K3	$21.35 \pm 20.68$	5.7	0.000	
	K4	$25.64 \pm 26.58$	9.2	0.000	
$\text{PM}_{2.5}$ ( $\mu\text{g}/\text{m}^3$ )	L1	$16.79 \pm 16.21$	3	0.000	0.000
	L2	$17.98 \pm 20.03$	3.6	0.000	
	L3	$24.98 \pm 30.43$	3.3	0.002	
	L4	$15.41 \pm 18.66$	4.7	0.000	
	L5	$17.95 \pm 18.54$	4.1	0.000	

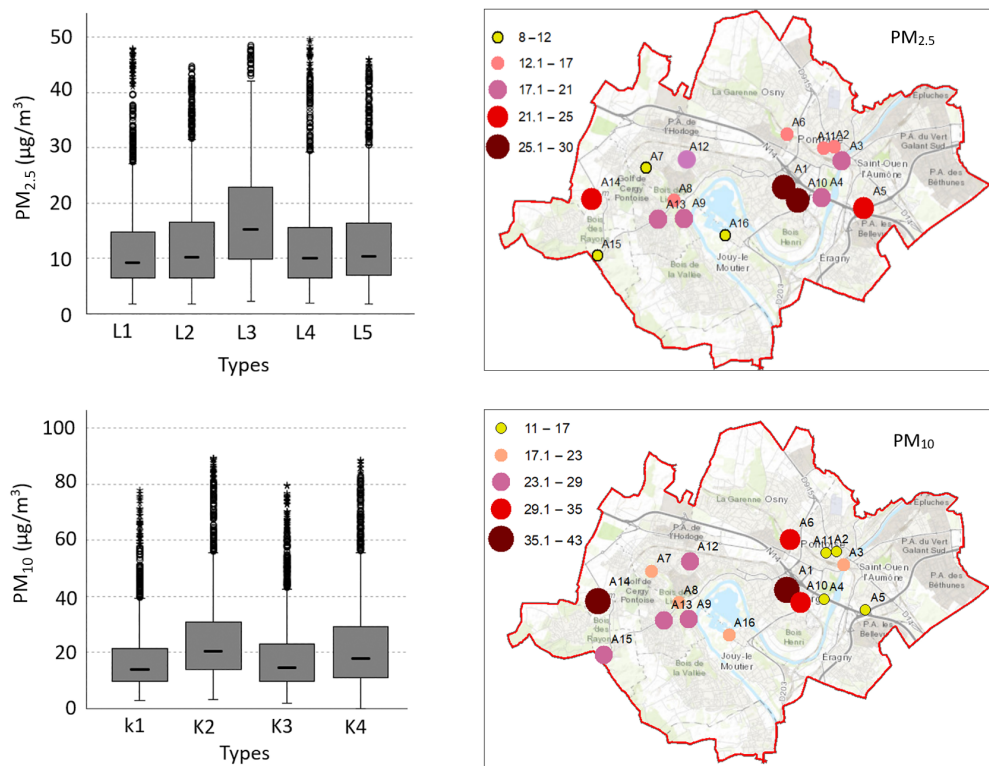
Note: Kolmogorov–Smirnov distance (K–S) = maximum cumulative distance between the histogram of measured data and the Gaussian distribution curve. p: Probability value (data from April 8 to June 6, 2022).

**FIGURE 5** Box plot of  $\text{NO}_2$  concentrations (ppb) measured in each group and spatial distribution map of the average concentrations calculated in the 16 sites (data from April 8 to June 6, 2022).

(13 ppb daily average) due to this proximity of placement. However, the analysis of box plots from the Kruskal–Wallis test identifies three concentration zones for  $\text{NO}_2$ : critical, very high, and high (Figure 5). Group D4 is classified as a critical concentration site, with an average of  $69.64 \pm 27.23$  ppb. It represents a sampling location situated within a sports complex near the bustling “a15” highway in the city. The “a15” highway handles around 158,000 vehicles daily as it traverses the urban area of Cergy-Pontoise (Drieat, 2020). Groups D2, D3, and D5 are classified as very high concentration, with values of  $49.41 \pm 20.06$  ppb,  $46.99 \pm 19.46$  ppb, and  $52.53 \pm 16.7$  ppb, respectively. The urban forms in these sites

range from residential (four sites) to city centers with many commercial activities (six sites), a rural site, and a site within a large park. Except group D5, the spatial distribution of  $\text{NO}_2$  concentrations is quite homogeneous in these sites. Group D1 is considered a high concentration zone ( $40.38 \pm 18.25$  ppb). It corresponds to a site in the city center within the university campus (distant from traffic routes) and three peripheral residential sites. In these residential areas, traffic is significantly lower than in the central urban sectors (not exceeding 5750 vehicles per day). The city center site (A1 = 34.07 ppb) is characterized by heavy road traffic (Cergy Préfecture). However, sampling conducted at 77 m from the road reduces its

**FIGURE 6** Box plot of the concentrations ( $\mu\text{g}/\text{m}^3$ ) measured in each group and spatial distribution map of the average concentrations calculated in the 16 sites ( $\text{PM}_{2.5}$  at the top and  $\text{PM}_{10}$  at the bottom) (data from April 8 to June 6, 2022).



concentration by 19% compared with the nearest site (A10 = 41.85 ppb).

The analysis of topographic properties reveals two main factors affecting air quality: the Sky View factor and the flow/speed of road traffic. Indeed, despite a significant vehicle flux, pollution accumulation is reduced in areas with a significant opening to the sky. Urban sites with a low Sky View factor are often characterized by one-way traffic. Since the car flow is low, the recorded concentrations are mainly due to severely hindered air renewal.

### 3.1.3 | Distribution of particle pollution

The  $\text{PM}_{2.5}$  box plots reveal relatively similar concentrations within the L1, L2, and L4 groups ( $L1 = 16.79 \pm 16.21 \mu\text{g}/\text{m}^3$ ;  $L2 = 20.03 \pm 17.98 \mu\text{g}/\text{m}^3$ ;  $L4 = 18.66 \pm 15.41 \mu\text{g}/\text{m}^3$ ;  $L5 = 18.54 \pm 17.95 \mu\text{g}/\text{m}^3$ ) (Figure 6). However, the spatial distribution map of concentrations shows variations between sites, suggesting that within these three groups, although generally homogeneous, spatial concentration variation persists. It is noteworthy that the A5 site (N184/“a15” interchange) and the A14 site (rural area) exhibit elevated concentrations, ranging from 21.1 to 25  $\mu\text{g}/\text{m}^3$ . Their concentrations may be associated with traffic and natural substrates, particularly for the A14 site. The most extreme concentrations ( $30.43 \pm 24.98 \mu\text{g}/\text{m}^3$ ) are observed in the L3 group,

composed of a single site in the urban center of Cergy-Prefecture and the A1 site, also located in this city center. This is likely a result of the proximity to numerous heavily trafficked avenues, a major bus terminal with 19 lines serving over 77,000 passengers per day, and several construction sites nearby. Since 2019, the center of Cergy-Préfecture has been undergoing extensive redevelopment. The ongoing urbanization aims to completely transform the urban center, creating “the great center” by 2025, with 160,000  $\text{m}^2$  of new residential areas, a train hub, and over 16,000  $\text{m}^2$  of refurbished and extended commercial spaces, as well as renovated public spaces.

Regarding  $\text{PM}_{10}$  pollution, high concentrations were found in group K2 ( $31.96 \pm 30.68 \mu\text{g}/\text{m}^3$ ) (Figure 6). This group comprises two sites in the urban center of Cergy-Préfecture (one in the city center and the other on the university campus) and two peripheral sites (one in a rural area and the other in a peri-urban area at the bottom of a vegetated valley). On the outskirts of the city, pollution is mainly due to high pollen activity, which increases  $\text{PM}_{10}$  concentrations (Monnier et al., 2015; Rahman et al., 2019), while in the city center, pollution primarily comes from road traffic. Group K3 includes four residential sites where car traffic is limited to local residents and one site in the middle of an urban park. It also includes two sites in urban centers (one in Cergy-Saint Christophe and the other in Pontoise, near the banks of the Oise River). Group K4 corresponds to a site located at

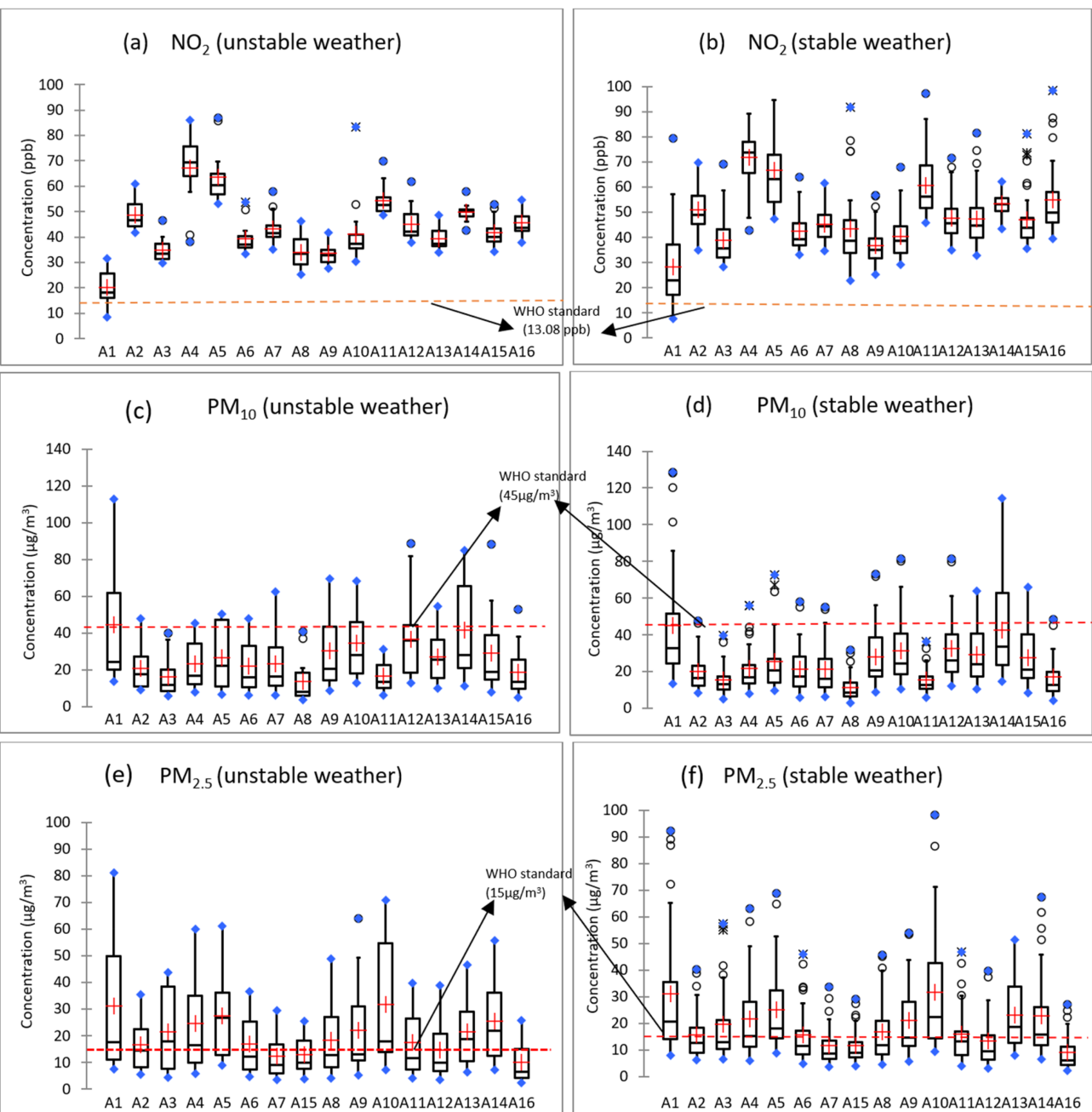


**FIGURE 7** Box plot of daily average concentrations ( $\text{NO}_2$ ,  $\text{PM}_{10}$ , and  $\text{PM}_{2.5}$ ) calculated on the 16 sampling sites in stable and unstable weather (data from April 8 to June 6, 2022).

the roundabout of the central square of the city of Vauréal, a city located on the western outskirts of the conurbation. Groups K3 and K4 have intermediate  $\text{PM}_{10}$  concentration levels ( $K3 = 21.35 \pm 20.68 \mu\text{g}/\text{m}^3$  and  $K4 = 25.64 \pm 26.58 \mu\text{g}/\text{m}^3$ ). The lowest concentration levels ( $19.28 \pm 16.18 \mu\text{g}/\text{m}^3$ ) are recorded in group K1, which consists of two sites in the urban center of the city of Pontoise (low road traffic), one site in a sports complex near the “a15” highway, and one site in a residential complex near the “N184”/“a15” interchange. For the latter two, the low concentration is due to the presence of

barriers (hedgerows and walls) established along these two busy traffic axes, preventing the propagation of  $\text{PM}_{10}$  toward residential areas. We demonstrated above that the sports complex near the “a15” highway (site A4) and the interchange between the “a15” highway and the “N184” are polluted with  $\text{NO}_2$  and  $\text{PM}_{2.5}$  (site A5). It can be concluded, therefore, that the hedgerow, which is a porous barrier, and the wall are only effective in the case of coarse particulate pollution ( $\text{PM}_{10}$ ). Furthermore, the low concentrations observed in group K1 can also be justified by the distance from pollen sources.

### 3.2 | Impact of weather types on PM<sub>10</sub>, PM<sub>2.5</sub>, and NO<sub>2</sub> concentrations

During the study period, we identified three types of weather using the method developed in Lagmiri and Dahech (2023): stable (often associated with anticyclonic situations), unstable (often associated with depression systems and weather fronts), and transitional weather (a meteorological period characterized by gradual changes from one weather type to another). Only the first two types are considered for assessing the state of air quality. Figure 7 highlights the relationship between the concentrations of the three pollutants and the considered weather conditions. We observe that the highest NO<sub>2</sub> concentrations occur during stable weather (Figure 7b). In fact, skies with low wind speeds govern the concentrations of atmospheric pollutants by reducing their dilution after emission. Unstable weather conditions increase dispersion and reduce pollutant concentrations at all monitoring stations (Figure 7a). Regardless of the weather type, the sampling sites show daily concentrations of NO<sub>2</sub> that significantly exceed the WHO standard (13.08 ppb or 25 µg/m<sup>3</sup>; daily average). This excess is closely linked to NO<sub>2</sub> emissions from vehicles and is favored by stable weather. The latter poses a higher risk of exposure because NO<sub>2</sub> gas, often emitted near the ground, remains trapped in the lower layers of the atmosphere.

Unlike gas pollution, particulate pollution (PM<sub>10</sub> and PM<sub>2.5</sub>) is higher during windy weather conditions (Figure 7c,e). Specifically, it is the concentrations of particles exceeding the median value that increase compared with stable weather (Figure 7d,f). Indeed, at wind speeds above 5 m/s, dust on the ground can be easily lifted, creating new particle pollution. Additionally, at this speed, long-distance wind transport is favored. The daily average concentrations of PM<sub>10</sub> in the third and fourth quartiles indicate that the majority of stations record less than 25% of values exceeding the WHO standard (45 µg/m<sup>3</sup>; daily average), regardless of the weather situation (Figure 7c,d). The only exception is found at the university campus and rural station (A1 and A14), where the percentage of exceedances varies from 38% to 35%. The box plots also show that some stations never exceed the standard (A3, A8, A11, and A16). The low automobile traffic or absence of circulation can account for the readings at stations A8, A11, and A16, while the importance of the Sky View factor, distance from pollen sources, and a probability of wet deposition (proximity to the Oise River) may be responsible for the rates recorded at station A3. Regarding PM<sub>2.5</sub> pollutant, concentrations above the third quartile show higher values during perturbed

weather. Noncompliance with the WHO standard (15 µg/m<sup>3</sup>; daily average) is observed in over 50% of the recordings for half of the stations during stable and unstable weather (Figure 7e,f).

### 3.3 | Weekly and diurnal cycle of pollutants

The weekly and diurnal cycles of the pollutants studied make it possible to distinguish the daily pollution regime (Figure 8). During the morning and evening rush hours, NO<sub>2</sub> concentrations are the highest (ranging from 70 to 115 ppb). At this time, traffic is active. On the “a15” highway (in group D4), the traffic flow is around 1345 vehicles/h, and the average speed drops from 110 to 70 km/h (data from DRIEAT, 2020). In the midday hours, concentrations decrease due to reduced emissions compared with peak hours (a decrease of up to 40 ppb in D4 group). Meteorological data on wind and atmospheric boundary layers (data from Météo France) have shown that the daytime wind speed and mixing layer height are on average higher than at night (a difference of 1.7 m/s for wind speed and 1.7 hPa for atmospheric height). This indicates higher mixing and dilution of NO<sub>2</sub> during the day. After the evening rush hour, concentrations slowly decrease until the early morning hours. Overall, they remain higher than during the day due to a shallow boundary layer. This hourly pattern is observed from Monday to Friday. During the weekend, the morning peak is reduced on Saturday and absent on Sunday. Similar results have been observed in other studies (Ben Romdhane, 2017; Dahech et al., 2022; Duché, 2014; Qin et al., 2004).

Like NO<sub>2</sub>, daily amplitudes of PM are clearly marked, showing that concentrations are also influenced by environmental conditions. The diurnal cycle has a high peak in the morning and a lighter peak in the late afternoon. This may be linked, in addition to road traffic, to the high pollen levels that occur particularly in the morning (Burki et al., 2019). According to Menut (1997), the morning transition marked by the disappearance of thermal inversion (during radiative conditions) at mid- and low latitudes is rapid and occurs shortly after sunrise, unlike the slow transition in the evening. Particles trapped during the night are rapidly re-injected at the surface in the morning (Hannah et al., 2021; Li et al., 2019).

The AirParif monitoring station (Ac) has the lowest PM<sub>10</sub> concentrations as it is installed at 6 meters in height, which is twice the height of our stations. Unlike NO<sub>2</sub>, PM concentrations exhibit a unique diurnal

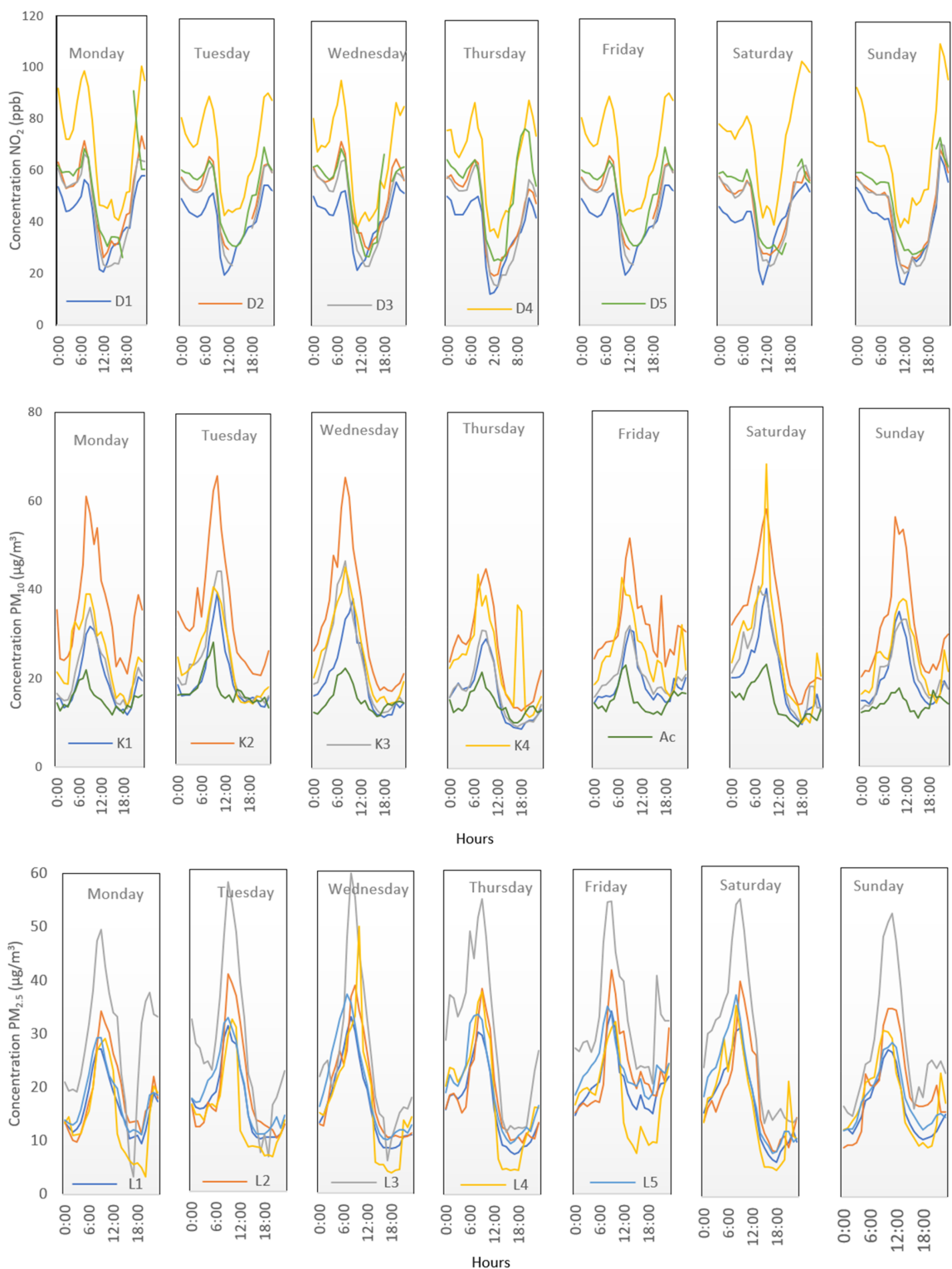


**FIGURE 8** Diurnal/weekly cycle of hourly averages of  $\text{NO}_2$  (ppb),  $\text{PM}_{10}$ , and  $\text{PM}_{2.5}$  ( $\mu\text{g}/\text{m}^3$ ) for the groups derived from the hierarchical cluster analysis; Ac on the  $\text{PM}_{10}$  graph represents data from April 8 to June 6, 2022.

variation, peaking during the day due to turbulence and pollen activity. While the diurnal cycle of  $\text{NO}_2$  and PM shows a bimodal pattern, the distinction between weekdays and weekends is rarely observed, suggesting a small impact on the weekly cycle of human activities.

### 3.4 | Spatial variability of pollution during morning peak hours

To inspect the spatial distribution of pollution of local origin, only the concentrations during stable weather are

**TABLE 4** Mean and standard deviation (SD) of NO<sub>2</sub> (ppb), PM<sub>10</sub>, and PM<sub>2.5</sub> ( $\mu\text{g}/\text{m}^3$ ) concentrations calculated during morning rush hours at the 16 sites; and correlation coefficient (*r*) calculated with respect to station A8 and Ac=Airparif (*x* represents the site number from 1 to 16) (data from April 8 to June 6, 2022).

PM <sub>2.5</sub>		PM <sub>10</sub>			NO <sub>2</sub>		
Site	Mean $\pm$ SD	Correlation ( <i>r</i> ) AX <sub>1-16</sub> /A8	Mean $\pm$ SD	Correlation ( <i>r</i> ) AX <sub>1-16</sub> /A8	Correlation ( <i>r</i> ) AX <sub>1-16</sub> /AC	Mean $\pm$ SD	Correlation ( <i>r</i> ) AX <sub>1-16</sub> /A8
A1	35 $\pm$ 30	0.77	45 $\pm$ 34	0.97	0.79	46 $\pm$ 22	0.66
A2	19 $\pm$ 13	0.85	29 $\pm$ 21	0.96	0.75	71 $\pm$ 12	0.58
A3	21 $\pm$ 15	0.75	13 $\pm$ 9	0.97	0.82	55 $\pm$ 9	0.47
A4	27 $\pm$ 21	0.85	34 $\pm$ 22	0.88	0.50	97 $\pm$ 20	0.41
A5	36 $\pm$ 27	0.96	61 $\pm$ 50	0.96	0.82	88 $\pm$ 25	0.39
A6	21 $\pm$ 16	0.83	21 $\pm$ 12	0.90	0.79	60 $\pm$ 8	0.63
A7	19 $\pm$ 14	0.82	36 $\pm$ 24	0.90	0.63	67 $\pm$ 9	0.64
A8	24 $\pm$ 20	1.00	22 $\pm$ 17	1.00	0.76	52 $\pm$ 9	1.00
A9	34 $\pm$ 26	0.92	26 $\pm$ 20	0.93	0.71	55 $\pm$ 11	0.74
A10	39 $\pm$ 33	0.81	24 $\pm$ 17	0.93	0.92	60 $\pm$ 15	0.59
A11	16 $\pm$ 14	0.68	18 $\pm$ 10	0.97	0.79	84 $\pm$ 13	0.46
A12	20 $\pm$ 18	0.97	42 $\pm$ 27	0.96	0.82	70 $\pm$ 14	0.44
A13	29 $\pm$ 22	0.95	17 $\pm$ 13	0.87	0.65	56 $\pm$ 9	0.62
A14	37 $\pm$ 31	0.96	44 $\pm$ 32	0.82	0.71	67 $\pm$ 8	0.32
A15	17 $\pm$ 11	0.94	24 $\pm$ 17	0.79	0.78	57 $\pm$ 10	0.31
A16	12 $\pm$ 10	0.97	22 $\pm$ 15	0.97	0.87	65 $\pm$ 10	0.72

taken into account. The results presented in Table 4 show that during morning rush hours, the highest average PM<sub>2.5</sub> and PM<sub>10</sub> concentrations were obtained at sites A1 (35 and 45  $\mu\text{g}/\text{m}^3$  respectively), A5 (36 and 61  $\mu\text{g}/\text{m}^3$  respectively), and A14 (37 and 44  $\mu\text{g}/\text{m}^3$  respectively). A high average concentration was also found at sites A9 and A10 for PM<sub>2.5</sub> (34 and 39  $\mu\text{g}/\text{m}^3$ , respectively) and at sites A7 and A12 for PM<sub>10</sub> (42  $\mu\text{g}/\text{m}^3$ ). The lowest concentrations are observed at sites A11, A15, and A16 for PM<sub>2.5</sub> and at sites A3, A11, and A13 for PM<sub>10</sub>. For each pollutant, the remaining stations have intermediate concentrations. The gaseous pollutant (NO<sub>2</sub>) is present in high concentrations at stations A4, A5, and A11. Conversely, stations A1, A3, A8, A9, A13, and A15 exhibit the lowest concentrations.

The correlation coefficients (*r*) were obtained by comparing the daily concentrations of the 16 sites with those of station A8 for the same measurement periods. This station was chosen for its proximity and residential properties similar to the AirParif reference station. For AirParif, only the correlation of the pollutant PM<sub>10</sub> was tested with the 16 “Ecosmart” stations because the data for the other pollutants were not available. The results show that PM<sub>2.5</sub> and PM<sub>10</sub> have better correlation coefficients than NO<sub>2</sub>. This quantitatively indicates that PM<sub>2.5</sub> and PM<sub>10</sub> are more uniformly distributed in the air than NO<sub>2</sub>. The

latter has correlation coefficients that vary mainly according to the density of road traffic, which differs according to neighborhoods. The PM<sub>10</sub> correlations calculated with respect to station A8 are slightly higher than those of AirParif. The difference may be due to the fact that the AirParif station is installed 6 meters above the ground, that is, 3 meters higher than the other stations.

### 3.5 | Spatial variability of pollution outside rush hours

The spatial variability of pollutants during stable weather at different times of the day was analyzed to provide new insights into air quality. Based on relative thresholds by pollutant and by period (morning 5 a.m.–12 p.m., afternoon 1 p.m.–5 p.m., and evening 9 p.m.–4 a.m.), the sites were classified into two groups: high concentration group and low concentration group. Based on Figure 9a, it can be observed that according to this classification, NO<sub>2</sub>, PM<sub>10</sub>, and PM<sub>2.5</sub> are not uniformly distributed among the sites. We noticed that the sites with lower concentrations and those with higher concentrations remained the same during the three studied periods, except for two sites for PM<sub>2.5</sub> and three sites for NO<sub>2</sub>, which changed their ranking in the afternoon. Although pollutants tend to

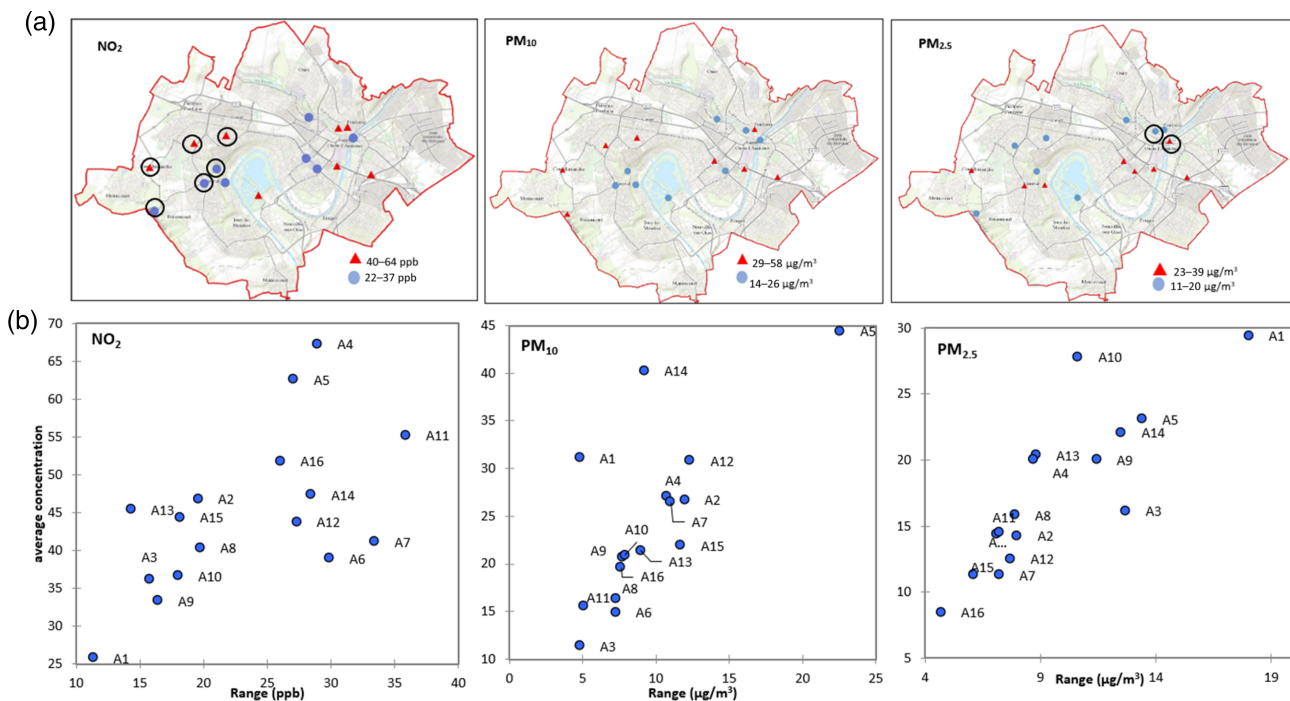


**FIGURE 9** (a) Maps of sites classified as high concentrations (red triangles) and low concentrations (blue circles) using pollutant-specific thresholds for the morning period (excluding peak hours). The sites enclosed in black represent those that changed classification in the afternoon. (b) Scatter plot identifying sites with the highest variability (large extent) and the least variability (low extent) over time (data from April 8 to June 6, 2022).

maintain a general pattern of distribution, their concentrations vary at different times of the day (morning, afternoon, and evening). NO<sub>2</sub> concentrations are higher in the evening (averaging 57.5 ppb), while PM concentrations are higher in the morning (averaging 22.87 µg/m<sup>3</sup> for PM<sub>2.5</sub> and 30.24 µg/m<sup>3</sup> for PM<sub>10</sub>). This result is expected and corroborates the findings of the section on the weekly and diurnal cycle of pollutants. As explained earlier, nocturnal concentrations of NO<sub>2</sub> are due to nighttime stability, while diurnal concentrations of particles (PM) are influenced by turbulence and pollen activity during the day. The lowest concentrations for NO<sub>2</sub> (averaging 36.41 µg/m<sup>3</sup>) are recorded in the afternoon, while the particulate matter shows relatively similar average values between the evening and the afternoon (13.41 µg/m<sup>3</sup> for PM<sub>2.5</sub> and 21.23 µg/m<sup>3</sup> for PM<sub>10</sub>—afternoon values).

To provide further insight into the spatial disparities, we calculated the average and range for each site, representing the difference between the highest and lowest values observed during three distinct periods. These results enable the identification of sites that exhibit consistent concentrations over time, indicating that the dominant factors influencing pollutant levels are specific to each location, rather than being influenced by temporal changes. Figure 9b illustrates the following trends:

Site A1 consistently exhibits low levels of NO<sub>2</sub>; A3 and A11 have lower PM<sub>10</sub> concentrations, while A16 and A15 show lower PM<sub>2.5</sub> levels. On the other hand, A13 consistently records high NO<sub>2</sub> concentrations, and A1 has consistently high PM<sub>10</sub> levels. The remaining sites display fluctuations in ranking depending on the time of day, implying significant temporal variations in pollutant concentrations. Analyzing the range values distribution, we found that sites A11 and A7 (NO<sub>2</sub>), A5 (PM<sub>10</sub>), and A1 (PM<sub>2.5</sub>) experience the most variability during the day.

Overall, stations with the most variable concentrations of NO<sub>2</sub> and PM<sub>10</sub> tended to be located near major highways, in two-way residential areas, in an urban center with narrow roads, and a boundary speed of 10 km/h, as well as in the large park of the urban area located near a peri-urban axis with heavy traffic (the latter only applies to NO<sub>2</sub>). Overall, stations with the most variable concentrations of NO<sub>2</sub> and PM<sub>10</sub> tend to be located close to major roadways, in residential areas with two-way traffic, in the urban center with narrow intersecting roads and a speed limit of 10 km/h, as well as in the large park of the urban area located near a heavily trafficked suburban route (the latter applies only to NO<sub>2</sub>). In contrast, the least variable sites are typically located away from roads, within the urban center with significant Skye Vieu Factor, and to the west in residential areas with one-way

traffic. As for  $\text{PM}_{2.5}$ , the concentrations are most variable near high-speed traffic lanes, the Vauréal roundabout, and construction sites, while they remain more stable in residential areas, the urban park, and within canyon streets.

## 4 | DISCUSSION

The results of this study show that spatial differences in concentrations are particularly influenced by urban typology.  $\text{NO}_2$  concentrations are high in the main access and exit routes of the urban area. They are also elevated in the city center as the streets become narrower. When the Sky View factor is significant, there is a reduction in concentrations even with significant road traffic in the city center. This is entirely consistent with the findings of Tang and Wang (2007), which demonstrated that the presence of narrower roads, complex road networks, and a higher density of intersections result in higher pollutant concentrations. Likewise, an 81% decrease in  $\text{NO}_2$  is observed between two sites with the same characteristics, except one that is located at the edge of the road and the other is situated 77 meters away. This helps identify the role of the distance to the road segment in spatial variability.  $\text{PM}_{10}$  pollution is particularly found in peripheral areas with vegetation and nonconcrete substrates and in the city center near construction sites. This result aligns with other studies that have reported similar findings (Dahech, 2007b; RAO, 2017). Low concentrations are found in sites close to highways but sheltered by obstacles such as hedges or walls. These elements, often located between high-traffic roads and residences, have a beneficial impact on reducing  $\text{PM}_{10}$  concentrations. This result is consistent with previous works (Baldauf et al., 2008; Hagler et al., 2012; Reiminger et al., 2020; Schulte et al., 2014). Therefore, it is recommended to implement such measures near densely populated urban areas to avoid exposure to  $\text{PM}_{10}$  along linear sources. The lack of efficiency in reducing  $\text{PM}_{2.5}$  and  $\text{NO}_2$  pollution is related to the properties of each type of obstacle. Even though hedges are considered effective windbreaks, their porous nature allows gas and fine particles to penetrate. As for the roadside wall line, previous studies (Bowker et al., 2007; Ning et al., 2010) have suggested that its presence generates a concentration-deficit zone immediately adjacent to the highway, followed by a surge in concentrations further downwind. In our study, we attribute high concentrations to the wall's action, which increases the vertical mixing of pollutants due to the diversion of airflow upwards. As  $\text{NO}_2$  and  $\text{PM}_{2.5}$  have low weight, they are vertically dispersed and then deposited away from the road, which could explain their lower

concentrations.  $\text{PM}_{2.5}$  distribution is more complex in urban forms compared with  $\text{PM}_{10}$  and  $\text{NO}_2$  because it comes from both biological and anthropogenic sources. It would be interesting in the future to study the  $\text{PM}_{2.5}/\text{PM}_{10}$  ratio to identify the sources of  $\text{PM}_{2.5}$  in a detailed manner. This approach could characterize  $\text{PM}_{2.5}$  concentrations based on land use, which cannot be identified using a simple map of  $\text{PM}_{2.5}$  distribution.

The differences in measured concentrations between day and night have established the important role played by meteorological conditions (mixing layer height and turbulence level) in the concentration of the three pollutants. Indeed, according to several studies, daytime heating of the air by the ground induces the formation of a convective boundary layer. Cooling of the ground by radiation during the night suppresses vertical eddies, leading to the existence of a stable nocturnal layer (Jin et al., 2021; Wang et al., 2021; Yuan et al., 2020). The common result of all these studies converges towards the fact that the insufficient development of the boundary layer disrupts the diffusion of pollutants and leads to their accumulation. However, in our study, this is true only for  $\text{NO}_2$ . Increased turbulence in the urban boundary layer during the day contributes to elevated levels of  $\text{PM}_{10}$  and  $\text{PM}_{2.5}$  through the lifting of dust from the ground and the movement of pollen during the spring. The impact of vertical and horizontal atmospheric stability is therefore variable and complex depending on the study area, season, and pollutant considered.

High concentrations during morning and late afternoon rush hours indicate that the sites are more affected by vehicle emissions, a finding supported by high noise levels. Regarding the weather types, this study shows that the population's exposure in the urban area is relatively high during stable weather for  $\text{NO}_2$  and during unsettled weather for particles in the spring. The daily limit for  $\text{NO}_2$  was not consistently adhered to during the observation period, meaning there was nearly constant exposure to exceedances, particularly during stable weather. Regarding particulate pollution, noncompliance with WHO standards is more noticeable for  $\text{PM}_{2.5}$  than for  $\text{PM}_{10}$ .

To complement these results, a detailed analysis of the spatiotemporal variation during stable weather is conducted to specifically identify locally originated pollution, using the method of mobile measurements. This allows tracking variations in air quality levels for different time periods and extracting spatial behavior. During the morning rush hours, the difference in concentrations between stations indicates traffic is the dominant factor contributing to the spatial behavior of  $\text{NO}_2$ . In contrast, the results show that PM is a multisource pollutant. For

instance, in the case of station A1, particulate pollution ( $PM_{10}$  and  $PM_{2.5}$ ) is higher even though this station is not immediately exposed to traffic emissions. This suggests that besides traffic, this site is impacted by another pollution source (construction sites) and probably wood heating during the winter. Site-averaged results (Figure 9) tend to obscure these differences in particulate pollution concentrations during morning rush hours but remained representative regarding gaseous pollution. Analyzing time-series data for morning, afternoon, and night periods reveals that sites with the highest variability throughout the day are those where pollution is attributed to more anthropogenic factors, combining mobile emission sources with unfavorable urban forms for dispersion (e.g., narrow streets). The least variable sites correspond to locations where urban morphology is designed to reduce traffic flow, either with one-way streets or wide boulevards that do not favor pollutant accumulation. This study confirms the findings of previous research, explaining that concentrations in complex urban environments have a relationship with traffic (Arkouli et al., 2010; Dahech & Rekik, 2012; Wolf et al., 2019).

This study, in light of the explanations described above, highlights that even in an urban area created and developed only 50 years ago, adhering to well-thought-out architectural standards, the problem of pollution persists. This work provides a deeper understanding of the dynamics within a recent urban area lacking fine-scale data.

## 5 | CONCLUSION

Monitoring air quality in urban areas is challenging as regulatory monitoring networks are scarce due to high investment costs. Technological advancements have led to widespread adoption of innovative detection instruments, such as “Ecosmart” sensors, enabling the acquisition of air quality data at high spatial resolution. By installing a network of 16 such sensors, we were able to achieve sufficient coverage of the Cergy-Pontoise urban area, allowing us to create pollution maps for different weather conditions between April and early June 2022. Although it may not be considered dense enough from a geostatistical point of view, having such fine coverage for an 89-km<sup>2</sup> conurbation is quite exceptional. The results of this study revealed that air quality is affected by a combination of traffic, urban design, and meteorological variables. The findings also indicate that a comprehensive spatiotemporal model is necessary to characterize short-term peaks and identify the most or least variable sites throughout the day. The data presented in this study

could play a crucial role in developing a mesoscale pollution control strategy.

In our future work, we will focus on a hybrid system that combines modeling and continuous monitoring using a denser sensor network to fill the coverage gaps between sampling sites. The aim is to better understand the various factors influencing concentrations at a fine scale and explore mitigation measures through urban design.

## AUTHOR CONTRIBUTIONS

**Souad Lagmiri:** Formal analysis (equal); funding acquisition (equal); methodology (equal); writing – original draft (equal); writing – review and editing (equal). **Salem Dahech:** Data curation (equal); funding acquisition (equal); methodology (equal); writing – review and editing (equal).

## ACKNOWLEDGEMENTS

The authors appreciate the anonymous reviewers for the critical comments that have helped improve this manuscript. The authors would like to thank the Interdepartmental Association for the Management of the Automatic Air Pollution Monitoring and Alert Network in the Île-de-France region (AirParif) and the National Oceanic and Atmospheric Administration (NOAA) for making the dataset available.

## FUNDING INFORMATION

This work was supported by DIM Qi2 program of the Île-de-France Region, the technical and financial support of the Cergy-Pontoise Conurbation, and the French Ministry of Higher Education and Research via the “Social Sciences” doctoral school (ED 624) (University of Paris).

## CONFLICT OF INTEREST STATEMENT

The authors declare no conflict of interest. All opinions, findings, and conclusions expressed in this article are those of the authors and do not reflect the views of the various funders.

## DATA AVAILABILITY STATEMENT

The data in this study are available from the corresponding author upon request ([souad.lagmiri@gmail.com](mailto:souad.lagmiri@gmail.com)).

## ORCID

Souad Lagmiri  <https://orcid.org/0009-0000-2777-9702>

## REFERENCES

- Alary, R., Donati, J. & Viellard, H. (1995) La pollution automobile à Paris influence du trafic et des conditions météorologiques. *Science of the Total Environment*, 169(1–3), 53–61. Available from: [https://doi.org/10.1016/0048-9697\(95\)04632-B](https://doi.org/10.1016/0048-9697(95)04632-B)

- Arkouli, M., Ulke, A.G., Endlicher, W., Baumbach, G., Schultz, E., Vogt, U. et al. (2010) Distribution and temporal behavior of particulate matter over the urban area of Buenos Aires. *Atmospheric Pollution Research*, 1, 1–8. Available from: <https://doi.org/10.5094/APR.2010.001>
- Balczó, M., Gromke, C. & Ruck, B. (2009) Numerical modeling of flow and pollutant dispersion in street canyons with tree planting. *Meteorologische Zeitschrift*, 18(2), 197–206. Available from: <https://doi.org/10.1127/0941-2948/2009/0361>
- Baldauf, R., Thoma, E., Khlystov, A., Isakov, V., Bowker, G., Long, T. et al. (2008) Impacts of noise barriers on near-road air quality. *Atmospheric Environment*, 42(32), 7502–7507. Available from: <https://doi.org/10.1016/j.atmosenv.2008.05.051>
- Ben Romdhane, S. (2017) Effets du climat et de la pollution de l'air sur la santé respiratoire à Tunis. Thèse de doctorat en géographie. Université Paris.
- Bowker, G.E., Baldauf, R., Isakov, V., Khlystov, A. & Petersen, W. (2007) The effects of roadside structures on the transport and dispersion of ultrafine particles from highways. *Atmospheric Environment*, 41(37), 8128–8139. Available from: <https://doi.org/10.1016/j.atmosenv.2007.06.064>
- Bozó, L., Labancz, K. & Steib, R. (2006) Estimation of air pollution in the year 2010 based on dynamical model calculations. *Proceedings of the Scientific Days in Meteorology*, Hungarian Meteorological Service, Budapest (pp. 207–215) (in Hungarian).
- Burki, C., Šikoparija, B., Thibaudon, M., Oliver, G., Magyar, D., Udvárdy, O. et al. (2019) Artificial neural networks can be used for *Ambrosia* pollen emission parameterization in COSMO-ART. *Atmospheric Environment*, 218, 116969. Available from: <https://doi.org/10.1016/j.atmosenv.2019.116969>
- Carteret, M., Andre, M. & Pasquier, A. (2014) Évaluation de la composition du parc automobile en Ile-de-France pour le calcul des émissions de polluants liés au trafic routier. *Pollution Atmosphérique: climat, santé, société*, 221, 14.
- Dahech, S. (2007b) Le vent à Sfax (Tunisie), impacts sur le climat et la pollution atmosphérique. Thèse de Doctorat, Université Paris Diderot, 309 pp.
- Dahech, S., Abdouleh, M.A. & Lagmiri, S. (2022) Spatiotemporal variation of air quality (PM and NO<sub>2</sub>) in southern Paris during COVID-19 lockdown periods. *Atmosphere*, 13(2), 289. Available from: <https://doi.org/10.3390/atmos13020289>
- Dahech, S. & Rekik, F. (2012) Trafic routier et pollution sonore à Sfax (Tunisie méridionale): étude pluridisciplinaire. *Pollution atmosphérique*, 215, 259–274. Available from: <https://doi.org/10.4267/pollution-atmospherique.185>
- DRIEAT (Direction Régionale et Interdépartementale de l'Environnement, de l'Aménagement et des Transports). (2020) Comptages routiers permanents (SIREDO) et temporaires (2020): résultats sur le département du Val d'Oise. Available at: <https://www.drieat.ile-de-france.developpement-durable.gouv.fr/>
- Duché, S. (2014) La pollution de l'air en région parisienne: exposition et perception sur les sites touristiques. Thèse de doctorat. Géographie. Université Paris-Diderot – Paris VII, 2013. Français. <https://theses.hal.science/tel-00840818v2>
- Euphrasie-Clotilde, L. (2018) Climatologie du transport des aérosols désertiques au-dessus de l'Atlantique vers la région Caraïbe. Thèse de doctorat, Université des Antilles, 213. Available at: <https://api.semanticscholar.org/CorpusID:217251502>
- Hagler, G.S.W., Lin, M.Y., Khlystov, A., Baldauf, R.W., Isakov, V., Faircloth, J. et al. (2012) Field investigation of roadside vegetative and structural barrier impact on near-road ultrafine particle concentrations under a variety of wind conditions. *Science of the Total Environment*, 419, 7–15. Available from: <https://doi.org/10.1016/j.scitotenv.2011.12.002>
- Hannah, G.M., Dirks, K.N., Neverman, A.J., Ian, M.K. & Salmon, J.A. (2021) The relationship between Brown haze, atmospheric boundary layer structure, and air pollution in an urban area of complex coastal terrain. *Atmospheric Pollution Research*, 12(5), 101057. Available from: <https://doi.org/10.1016/j.apr.2021.101057>
- Hoek, G., Beelen, R., de Hoogh, K., Vienneau, D., Gulliver, J., Fischer, P. et al. (2008) A review of land-use regression models to assess spatial variation of outdoor air pollution. *Atmospheric Environment*, 42(33), 7561–7578. Available from: <https://doi.org/10.1016/j.atmosenv.2008.05.057>
- IAU Île de France. (2019) CA Cergy-Pontoise Chiffre clés. Available from: <https://www.cergypontoise.fr/chiffres-cles>.
- INSEE (L'Institut National de la Statistique et des Etudes Economiques). (2019) Recensement de la pollution (2019): résultats sur le territoire de l'agglomération de Cergy-Pontoise. Available at: <https://www.insee.fr/fr/accueil>
- Jin, X., Cai, X., Yu, M., Wang, X., Song, Y., Kang, L. et al. (2021) Mesoscale structure of the atmospheric boundary layer and its impact on regional air pollution: a case study. *Atmospheric Environment*, 258, 118511. Available from: <https://doi.org/10.1016/j.atmosenv.2021.118511>
- Jonhson, M., Isakov, V., Touma, J.S., Mukerjee, S. & Ozkaynak, H. (2010) Evaluation of land-use regression models used to predict air quality concentrations in an urban area. *Atmospheric Environment*, 44(30), 3660–3668. Available from: <https://doi.org/10.1016/j.atmosenv.2010.06.041>
- Krewski, D., Jerrett, M., Burnett, R.T., Ma, R., Hughes, E., Shi, Y. et al. (2009) Extended follow-up and spatial analysis of the American Cancer Society study linking particulate air pollution and mortality. *Research Report Health Effects Institute*, 140, 5–114; discussion 115–36.
- Lagmiri, S. & Dahech, S. (2023) Weather types and their influence on PM<sub>10</sub> and O<sub>3</sub> urban concentrations in the Cergy-Pontoise conurbation. *Journal of Applied Meteorology and Climatology*, 62, 549–561. Available from: <https://doi.org/10.1175/JAMC-D-22-0161>
- Lasserre, F. (2006) Modélisation du cycle d'aérosols naturels et anthropiques en Asie orientale. Interfaces continentales, environnement. Université Blaise Pascal – Clermont-Ferrand II, 2006. Français.
- Li, X., Hu, X.-M., Ma, Y., Wang, Y., Li, L. & Zhao, Z. (2019) Impact of planetary boundary layer structure on the formation and evolution of air-pollution episodes in Shenyang, Northeast China. *Atmospheric Environment*, 214, 116850. Available from: <https://doi.org/10.1016/j.atmosenv.2019.116850>
- Liu, Y., He, K.B., Li, S.S., Wang, Z.X., Christiani, D.C. & Koutrakis, P. (2012) A statistical model to evaluate the effectiveness of PM<sub>2.5</sub> emissions control during the Beijing 2008

- Olympic games. *Environment International*, 44, 100–105. Available from: <https://doi.org/10.1016/j.envint.2012.02.003>
- Menut, L. (1997) Etude expérimentale et théorique de la couche limite atmosphérique en agglomération parisienne. Océan, Atmosphère. Université Pierre et Marie Curie – Paris VI, 1997. Français.
- Misra, P., Imasu, R. & Takeuchi, W. (2019) Impact of urban growth on air quality in Indian cities using hierarchical Bayesian approach. *Atmosphere*, 10, 517. Available from: <https://doi.org/10.3390/atmos10090517>
- Monnier, S., Thibaudon, M., Besancenot, J.-P. & Michelot, N. (2015) Air pollution, pollen, and pollinosis: another look at the pollution episode of March 2014 in France. *Atmospheric pollution*, 157–164, 25.
- Naughton, O., Donnelly, A., Nolan, P., Pilla, F., Misstear, B.D. & Broderick, B. (2018) A land use regression model for explaining spatial variation in air pollution levels using a wind sector based approach. *Science of the Total Environment*, 630, 1324–1334.
- Nicolas, J.-P. (1996) Ville, transports et environnement. Contributions relatives des paramètres du trafic routier affectant la pollution sonore et atmosphérique en milieu urbain. Sciences de l'Homme et Société. Université Lumière – Lyon II, 1996. Français.
- Ning, Z., Hudda, N., Daher, N., Kam, W., Herner, J., Kozawa, K. et al. (2010) Impact of roadside noise barriers on particle size distributions and pollutants concentrations near freeways. *Atmospheric Environment*, 44, 3118–3127. Available from: <https://doi.org/10.1016/j.atmosenv.2010.05.033>
- Pepe, N., Pirovano, G., Lonati, G., Balzarini, A., Toppetti, A., Riva, G.M. et al. (2016) Development and application of a high resolution hybrid modelling system for the evaluation of urban air quality. *Atmospheric Environment*, 141, 297–311. Available from: <https://doi.org/10.1016/j.atmosenv.2016.06.071>
- PPA. (2013) Plan de Protection de l'Atmosphère pour l'Île-de-France. Arrêté inter-préfectoral.
- Prospero, J., Glaccum, R. & Nees, R. (1981) Transport atmosphérique de la poussière du sol de l'Afrique vers l'Amérique du Sud. *Nature*, 289, 570–572. Available from: <https://doi.org/10.1038/289570a0>
- Qin, Y., Tonnesen, G.S. & Wang, Z. (2004) Weekend/weekday differences of ozone, NO<sub>x</sub>, Co, VOCs, PM<sub>10</sub> and the light scatter during ozone season in Southern California. *Atmospheric Environment*, 38, 3069–3087. Available from: <https://doi.org/10.1016/j.atmosenv.2004.01.035>
- Rahman, A., Luo, C., Khan, M.H.R., Ke, J., Thilakanayaka, V. & Kumar, S. (2019) Influence of atmospheric PM<sub>2.5</sub>, PM<sub>10</sub>, O<sub>3</sub>, CO, NO<sub>2</sub>, SO<sub>2</sub>, and meteorological factors on the concentration of airborne pollen in Guangzhou, China. *Atmospheric Environment*, 212, 290–304.
- RAO NIMRA. (2017) *Air quality monitoring of PM<sub>2.5</sub> and PM<sub>10</sub> at construction sites of Lahore*. Roll No: 171651041.
- Reiminger, N., Jurado, X., Vazquez, J., Wemmert, C., Blond, N., Dufresne, M. et al. (2020) Effects of wind speed and atmospheric stability on the air pollution reduction rate induced by noise barriers. *Journal of Wind Engineering and Industrial Aerodynamics*, 200, 104160. Available from: <https://doi.org/10.1016/j.jweia.2020.104160>
- Schulte, N., Snyder, M., Isakov, V., Heist, D. & Venkatram, A. (2014) Effects of solid barriers on dispersion of roadway emissions. *Atmospheric Environment*, 97, 286–295. Available from: <https://doi.org/10.1016/j.atmosenv.2014.08.026>
- Sindosi, O.A., Katsoulis, B.D. & Bartzokas, A. (2003) An objective definition of air mass types affecting athens, Greece: the corresponding atmospheric pressure patterns and air pollution levels. *Environmental Technology*, 24(8), 947–962. Available from: <https://doi.org/10.1080/09593330309385633>
- Spinelle, L., Mantelle, C., Marchand, C., Herbin, B., Crunaire, S. & Redon, N. (2020) *Résultats du premier essai national d'aptitude des capteurs (EAµC) pour la surveillance de la qualité de l'air, LCSQA*. Laboratoire Central de Surveillance de la Qualité de l'Air, p. 9. <https://www.lcsqa.org/fr/rapport/resultats-du-premier-essai-national-daptitude-des-micro-capteurs-eamc-pour-la-surveillance> [Accessed 10 October 2022].
- Tang, U.W. & Wang, Z.S. (2007) Influences of urban forms on traffic-induced noise and air pollution: results from a modelling system. *Environmental Modelling and Software*, 22(12), 1750–1764. Available from: <https://doi.org/10.1016/j.envsoft.2007.02.003>
- Ung, A. (2003) Cartographie de la pollution atmosphérique en milieu urbain à l'aide de données multisources. Physique [physics]. École Nationale Supérieure des Mines de Paris, 2003. Français.
- Wang, M., Tang, G., Liu, Y., Ma, M., Yu, M., Hu, B. et al. (2021) The difference in the boundary layer height between urban and suburban areas in Beijing and its implications for air pollution. *Atmospheric Environment*, 260, 118552. Available from: <https://doi.org/10.1016/j.atmosenv.2021.118552>
- Weidinger, T., Baranka, G., Makra, L. & Gyongyosi, A.Z. (2010) *Urban air quality, long term trends and road traffic air pollution modeling of szeged, urban transport and hybrid vehicles*. Urban Transport and Hybrid Vehicles. Available at: <http://dx.doi.org/10.5772/10180>
- Weinmayr, G., Hennig, F., Fuks, K., Nonnemacher, M., Jakobs, H., Möhlenkamp, S. et al. (2015) Long-term exposure to fine particulate matter and incidence of type 2 diabetes mellitus in a cohort study: effects of total and traffic-specific air pollution. *Environmental Health*, 14, 53. Available from: <https://doi.org/10.1186/s12940-015-0031-x>
- Wolf, T., Pettersson, L.H. & Esau, I. (2019) A very high-resolution assessment and modelling of urban air quality. *Atmospheric Chemistry and Physics*, 20, 625–647. Available from: <https://doi.org/10.5194/acp-20-625-2020>
- Wolf-Benning, U., Draheim, T. & Endlicher, W. (2009) Spatial and temporal differences of particulate matter in Berlin. *International Journal of Environment and Waste Management*, 4(1/2), 3–16. Available from: <https://doi.org/10.1504/IJEWM.2009.026880>
- Xing, J., Mathur, R., Pleim, J., Hogrefe, C., Gan, C.M., Wong, D.C. et al. (2015) Observations and modeling of air quality trends over 1990–2010 across the Northern Hemisphere: China, the United States and Europe. *Atmospheric Chemistry and Physics*, 15(5), 2723–2747.
- Xing, Y.F., Xu, Y.H., Shi, M.H. & Lian, Y.X. (2016) The impact of PM<sub>2.5</sub> on the human respiratory system. *Journal of Thoracic*

*Disease*, 8(1), E69. Available from: <https://doi.org/10.3978/j.issn.2072-1439.2016.01.19>

Yuan, Z., Qin, J., Zheng, X. & Mbululo, Y. (2020) The relationship between atmospheric circulation, boundary layer and near-surface turbulence in severe fog-haze pollution periods. *Journal of Atmospheric and Solar-Terrestrial Physics*, 200, 105216. Available from: <https://doi.org/10.1016/j.jastp.2020.105216>

**How to cite this article:** Lagmiri, S., & Dahech, S. (2024). Distribution of PM<sub>10</sub>, PM<sub>2.5</sub>, and NO<sub>2</sub> in the Cergy-Pontoise urban area (France).

*Meteorological Applications*, 31(4), e2223. <https://doi.org/10.1002/met.2223>